Temporal Accumulation of First-Order Linearization Error for Semi-Lagrangian Passive Advection

MONIQUE TANGUAY

Meteorological Research Branch, Atmospheric Environment Service, Dorval, Quebec, Canada

SAROJA POLAVARAPU

Meteorological Research Branch, Atmospheric Environment Service, Downsview, Ontario, Canada

PIERRE GAUTHIER

Meteorological Research Branch, Atmospheric Environment Service, Dorval, Quebec, Canada

(Manuscript received 31 May 1996, in final form 14 August 1996)

ABSTRACT

The tangent linear model (TLM) is obtained by linearizing the governing equations around a space- and time-dependent basic state referred to as the trajectory. The TLM describes to first-order the evolution of perturbations in a nonlinear model and it is now used widely in many applications including four-dimensional data assimilation. This paper is concerned with the difficulties that arise when developing the tangent linear model for a semi-Lagrangian integration scheme. By permitting larger time steps than those of Eulerian advection schemes, the semi-Lagrangian treatment of advection improves the model efficiency. However, a potential difficulty in linearizing the interpolation algorithms commonly used in semi-Lagrangian advection schemes has been described by Polavarapu et al., who showed that for infinitesimal perturbations, the tangent linear approximation of an interpolation scheme is correct *if and only if* the first derivative of the interpolator is continuous at every grid point. Here, this study is extended by considering the impact of temporally accumulating first-order linearization errors on the limit of validity of the tangent linear approximation due to the use of small but finite perturbations. The results of this paper are based on the examination of the passive advection problem. In particular, the impact of using incorrect interpolation schemes is studied as a function of scale and Courant number.

For a constant zonal wind leading to an integral value of the Courant number, the first-order linearization errors are seen to amplify linearly in time and to resemble the second-order derivative of the advected field for linear interpolation and the fourth-order derivative for cubic Lagrange interpolation. Solid-body rotation experiments on the sphere show that in situations where linear interpolation results in accurate integrations, the limit of validity of the TLM is nevertheless reduced. First-order cubic Lagrange linearization errors are smaller and affect small scales. For this to happen requires a wind configuration leading to a persistent integral value of the Courant number. Regions where sharp gradients of the advected tracer field are present are the most sensitive to this error, which is nevertheless observed to be small. Finally, passive tracers experiments driven by winds obtained from a shallow-water model integration confirm that higher-order interpolation schemes (whether correct or not) give similar negligible linearization errors since the probability of having the upstream point being located exactly on a grid point is vanishingly small.

1. Introduction

In recent years, there have been several studies that have shown that a 4D data assimilation scheme needs to take into account the dynamical constraints of the flow in its representation of the background error statistics. This can be done either implicitly as in a 4D variational scheme (4Dvar) (Thépaut et al. 1995) or explicitly as in the extended Kalman filter (Evensen 1992; Gauthier et al. 1993; Daley 1995) (see Courtier et al. 1993 for a review of the literature). Both approaches make use of the tangent linear approximation by assuming that the evolution in time of a perturbed model state caused by a small change to the initial conditions can be described by the tangent linear model (TLM), obtained by linearizing the model's equations around a time- and space-dependent reference state.

Referring to LeDimet and Talagrand (1986), a 4Dvar assimilation proceeds iteratively by minimizing a functional measuring the misfit between observations and a model solution obtained from given initial conditions. This requires the gradient of the functional with respect to changes in the initial conditions that can be obtained

Corresponding author address: Dr. Monique Tanguay, Recherche en Prevision Numerique, 2121, Route Trans-canadienne No. 508, Dorval, PQ H9P 1J3 Canada.

from a single backward integration of the adjoint of the TLM. In the extended Kalman filter, the TLM is used explicitly to integrate the forecast error covariances. In predictability studies, both the adjoint and the TLM are needed to obtain the singular vectors that describe those changes to the initial conditions that would lead to the most important error growth over a given finite period of time (Lacarra and Talagrand 1988). In all three applications, one must be aware that there is a limit of validity to the tangent linear approximation, which is not always easy to establish (see Tanguay et al. 1995 and references therein).

The very definition of the TLM assumes the model to be continuously differentiable with respect to changes in the initial conditions. Many physical parameterization packages introduce threshold processes that clearly make the model nondifferentiable. This problem has been discussed by Vukicevic and Errico (1993), Zupanski (1993), Zou et al. (1993), and Bao and Kuo (1995), for example. Similar difficulties are encountered when trying to develop the TLM for some numerical algorithms involving discrete processes that are not differentiable. This occurs, for instance, in semi-implicit models when a semi-Lagrangian treatment of advection is employed (Robert et al. 1985). Such difficulties were first pointed out by Li et al. (1993) and Ménard (1994), who have suggested that the limit of validity of the TLM could be reduced in regions where large gradients in the flow are combined with strong advection and that this may impose an additional restriction on the time step. Recently, Polavarapu et al. (1996a) have shown that in the limit of infinitesimal perturbations, the tangent linear approximation to an interpolation scheme is correct *if and only if* the first derivative of the interpolator is continuous at every grid point. This condition is what it takes to make the interpolation differentiable. In addition, for nondifferentiable interpolation of higher order accuracy, the amplitude of the first-order linearization error was shown to be smaller.

The study of Polavarapu et al. (1996a) considered only the case of infinitesimal perturbations and those situations occur only with a vanishingly small probability as $\Delta t \to 0$. In practice, finite time steps are used and thus such situations can occur. It then becomes important to know whether this can cause significant problems in the course of an integration when more dynamically realistic conditions are employed. The impact of accumulating this linearization error in time will be looked at by choosing a flow configuration that can be considered to be the worst case: a flow with constant velocity for which the upstream locations of *every* grid point can be made to lie exactly on another grid point by properly choosing the time step.

In section 2, the advection problem is stated for the case of solid-body rotation on the globe and a one-dimensional analysis is presented for the linearization of a semi-Lagrangian scheme using exact interpolation. In section 3, numerical interpolation is included in the analysis. In section 4, selected interpolation schemes are studied and the associated linearization errors over a fixed time interval are derived as a function of spatial scale and Courant number. In section 5, numerical examples illustrating properties of the errors are presented in the context of solid body rotation experiments on the globe. Semi-Lagrangian passive tracer experiments with predetermined winds are also presented and the impact of using higher-order interpolation schemes is investigated. A summary of the results and conclusions are presented in section 6.

2. Linearization of semi-Lagrangian passive advection: Exact interpolation

Referring to Ritchie (1987), the two-dimensional advection of a passive tracer on the sphere can be written as

$$\frac{d}{dt}F[\mathbf{r}(t), t] = 0, \tag{1}$$

where the material derivative is

$$\frac{d}{dt}(\ ) = \frac{\partial}{\partial t}(\ ) + \mathbf{v}_H \cdot \boldsymbol{\nabla}_H(\ ),$$

with $\mathbf{r}(t)$, the position vector as a function of time t and $\mathbf{v}_H$ the horizontal wind vector advecting a scalar field F. In longitude–latitude (λ, θ) coordinates, (1) takes the form

$$\frac{\partial F}{\partial t} = \frac{-1}{\cos^2\theta}\left(U\frac{\partial F}{\partial \lambda} + V\cos\theta\frac{\partial F}{\partial \theta}\right) \tag{2}$$

in which the zonal wind component u and the meridional wind component v are converted to model wind images $(U,V) = [(u/a)\cos\theta, (v/a)\cos\theta]$ with a, the radius of the earth.

We now consider the wind field to be that associated with a rotation at constant angular velocity ω about an axis passing through the center of the earth and a point P' on the earth's surface. In a spherical coordinates system (λ', θ') having its north pole at P', the advection equation reduces to the one-dimensional form

$$\frac{\partial F'}{\partial t} + \omega\frac{\partial F'}{\partial \lambda'} = 0. \tag{3}$$

For the sake of simplicity, the primes will now be omitted. This is referred to as an advection problem for a wind field associated with a solid-body rotation. The invariant nature of the problem makes it easy to show that the solution at a later time is

$$F(\lambda, t) = F_0(\lambda - \omega t), \tag{4}$$

where $F_0(\lambda)$ are the initial conditions. In a discretized form, the upstream point $(\lambda - \omega t)$ generally does not lie exactly on another grid point and $F_0(\lambda - \omega t)$ would be obtained from a spatial interpolation. Integration with

a semi-Lagrangian scheme produces the solution at a next time step Δt to be

$$F(\lambda, t + \Delta t) = F(\lambda - \omega\Delta t, t), \tag{5}$$

and $F(\lambda - \omega\Delta t, t)$ is obtained from a spatial interpolation. For now, F is assumed to be known exactly at $(\lambda - \omega\Delta t)$; the role of the interpolation will be looked at in the next section.

The model variables being F, the scalar field, and ω, the steady wind field, we will consider variations $\delta F_0(\lambda)$ in the initial conditions and constant variations, $\delta\omega$, of the wind field. The tangent linear model is then

$$\frac{\partial}{\partial t}\delta F + \omega\frac{\partial}{\partial\lambda}\delta F + \delta\omega\frac{\partial F}{\partial\lambda} = 0 \tag{6}$$

and its solution

$$\delta F(\lambda, t) = \delta F_0(\lambda - \omega t) - t\delta\omega\frac{d}{d\lambda}F_0(\lambda - \omega t).$$

The first term comes from advecting δF at the original upstream point $(\lambda - \omega t)$, while the second term comes from changes in the upstream position $\delta\omega t$ caused by perturbing the wind field: this leads to a linear growth in time of the perturbation. By contrast, the corresponding nonlinear variation would be

$$\begin{aligned}\Delta F &= F(F_0 + \delta F_0, \omega + \delta\omega) - F(F_0, \omega)\\ &= F_0[\lambda - (\omega + \delta\omega)t] + \delta F_0[\lambda - (\omega + \delta\omega)t]\\ &\quad - F(F_0, \omega)\end{aligned}$$

and a Taylor expansion in ω recovers the TLM solution at leading order. In this problem, what makes the TLM approximation inexact is the neglect of the perturbation in the upstream position for δF while this change is taken into account only approximately in the advection of F.

The semi-Lagrangian integration of (6) then yields

$$\delta F(\lambda, t + \Delta t) = \delta F(\lambda - \omega\Delta t, t) - \frac{\partial F}{\partial\lambda}(\lambda - \omega\Delta t, t)\delta\omega\Delta t. \tag{7}$$

Considering $t = n\Delta t$ and a uniform grid $\Delta\lambda$, a stability analysis is made by introducing monochromatic solutions of the form

$$F(\lambda, t) = F_0A^ne^{im\lambda}$$

in (5) and the response is given by

$$A = A(\alpha, m\Delta\lambda) = \exp(-i\alpha m\Delta\lambda), \tag{8}$$

where $\alpha = \omega\Delta t/\Delta\lambda$ is the Courant number and F_0 represents now the amplitude of the solution. For an Eulerian scheme, the time step would be limited by the CFL criterion but (8) shows that, in a semi-Lagrangian scheme, the maximum time step is no longer limited by the angular velocity.

The associated solution of the TLM due to variations in the initial amplitude, δF_0, and in the angular velocity, $\delta\omega$ (or equivalently in the Courant number $\delta\alpha$), can be written as

$$\delta_rF(\lambda, t) = \left[\delta_rF_0 + n\left(\frac{dA}{d\alpha}\frac{1}{A}\right)\delta\alpha\right], \tag{9}$$

where $\delta_rF = \delta F/F$ is the relative perturbation scaled with respect to F and, similarly, the relative perturbation to the initial conditions is $\delta_rF_0 = \delta F_0/F_0$. Since $A = \exp(-i\alpha m\Delta\lambda)$, then

$$\frac{dA}{d\alpha}\frac{1}{A} = -im\Delta\lambda$$

and (9) is equivalent to

$$\delta_rF(\lambda, t) = [\delta_rF_0 - (im)\delta\omega t]. \tag{10}$$

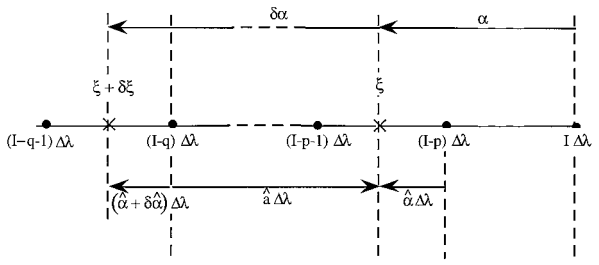

FIG. 1. Schematic diagram illustrating the parameters involved in the interpolation scheme on the longitude grid when evaluating the function value at the unperturbed and perturbed upstream locations as defined in section 3.

3. Linearization of semi-Lagrangian passive advection: Numerical interpolation

Generally, the upstream location $\xi = \lambda - \omega\Delta t$ will lie between grid points and the evaluation of $F(\lambda - \omega\Delta t, t)$ will require an interpolation since only gridpoint values of F are predicted. Stability and accuracy properties of the interpolating semi-Lagrangian advection scheme (e.g., Bates and McDonald 1982; McDonald 1984; Pudykiewicz and Staniforth 1984; Ritchie 1986, 1987) show very good phase speeds with little numerical dispersion, but there is some damping due to interpolation. This damping has been judged to be excessive for linear interpolation, which is not recommended for this reason. However, this damping is fortunately very scale selective for high-order interpolations [see Fig. 1 and 2 in McDonald (1984) and Fig. 1 in Pudykiewicz and Staniforth (1984)].

When interpolation is considered, semi-Lagrangian approximation at the point $\lambda = I\Delta\lambda$ is

$$F(\lambda, t + \Delta t) = P_{I-p}(\lambda - \omega\Delta t) \tag{11}$$

with P_{I-p}, an interpolating function over the interval $[I - p - 1, I - p)$. The interpolation schemes that will be considered here can be written in the form

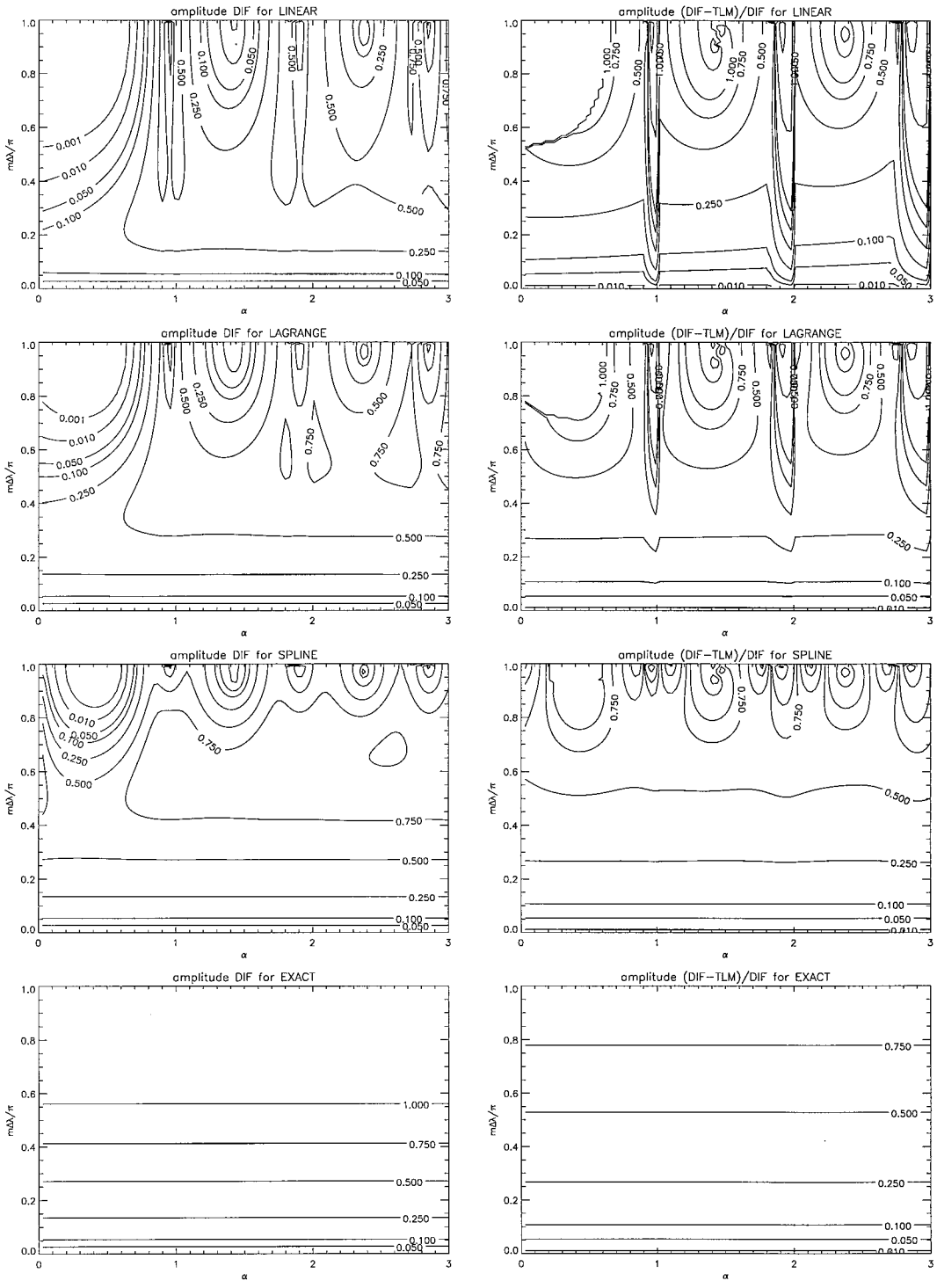

FIG. 2. Isolines of normalized amplitude of the nonlinear difference $\|\Delta F/F_0\|$ (left panel) and of the amplitude ratio of the discrepancy between the nonlinear difference and the associated TLM over the nonlinear difference [i.e., $\|(\Delta F - \delta F)/\Delta F\|$] (right panel) as a function of the Courant number α and of the nondimensional wavenumber $m\Delta\lambda/\pi$, for all four studied interpolation schemes. The isolines shown are 0.001, 0.01, 0.05, 0.1, 0.25, 0.5, 0.75, 1, 2, and 5.

$$P_{I-p}(\lambda - \omega\Delta t) = \hat{\alpha}F_{I-p-1} + (1 - \hat{\alpha})F_{I-p} + \frac{\Delta\lambda^2}{6}\{(\hat{\alpha}^3 - \hat{\alpha})F''_{I-p-1} + [(1 - \hat{\alpha})^3 - (1 - \hat{\alpha})]F''_{I-p}\} \quad (12)$$

as in Polavarapu et al. (1996a). Various interpolation schemes then differ only by the way the F'' are computed. For instance, $F'' \equiv 0$ corresponds to a linear interpolation while $F'' \neq 0$ could yield the cubic spline or the cubic Lagrange interpolations: those will be presented later. The index $(I - p)$ determines the interval $[(I - p - 1)\Delta\lambda, (I - p)\Delta\lambda)$ containing the upstream point. Consequently,

$$p = \text{int}(\alpha), \qquad \alpha \geq 0$$
$$p = \text{int}(\alpha - 1), \qquad \alpha < 0$$

and $p = \text{int}(x)$ is the first integer such that $p \leq x$. The displacement $\hat{\alpha}$ in between grid points is such that

$$\xi = (I - p)\Delta\lambda - \hat{\alpha}\Delta\lambda.$$

Unperturbed and perturbed upstream interpolation points could lie in different intervals depending on the size of $\delta\omega\Delta t$ (or equivalently $\delta\alpha$), as shown in Fig. 1. In such situations, as will be seen shortly, it then becomes important that the interpolation does not introduce discontinuities.

The tangent linear approximation to (9) is

$$\delta F(\lambda, t + \Delta t) = \delta P_{I-p}(\lambda - \omega\Delta t) - \frac{dP_{I-p}}{d\lambda}(\lambda - \omega\Delta t)\delta\omega\Delta t \quad (13)$$

with

$$\delta P_{I-p}(\lambda - \omega\Delta t) = \hat{\alpha}\delta F_{I-p-1} + (1 - \hat{\alpha})\delta F_{I-p} + \frac{\Delta\lambda^2}{6} \times \{(\hat{\alpha}^3 - \hat{\alpha})\delta F''_{I-p-1} + [(1 - \hat{\alpha})^3 - (1 - \hat{\alpha})]\delta F''_{I-p}\}$$

and

$$\frac{dP_{I-p}}{d\lambda}(\lambda - \omega\Delta t) = -\frac{1}{\Delta\lambda}\frac{dP_{I-p}}{d\hat{\alpha}}(\lambda - \omega\Delta t) = \frac{F_{I-p} - F_{I-p-1}}{\Delta\lambda} + \frac{\Delta\lambda}{6}\{(-3\hat{\alpha}^2 + 1)F''_{I-p-1} + [3(1 - \hat{\alpha})^2 - 1]F''_{I-p}\}.$$

This is the TLM for semi-Lagrangian passive advection with numerical interpolation included and is therefore an extension of (7).

Three interpolation schemes will be considered here: linear, cubic Lagrange, and cubic spline (see appendix A). As mentioned earlier, (12) is valid for all three: it suffices to introduce the appropriate definition for F''. As in the previous section, monochromatic solutions of the form $F = F_0A^n\exp(im\lambda)$ are introduced in (11) to obtain that

$$A = A(p, \hat{\alpha}, m\Delta\lambda) = [\hat{\alpha} + \gamma(\hat{\alpha}^3 - \hat{\alpha})]\exp[-i(p + 1)m\Delta\lambda] + \{(1 - \hat{\alpha}) + \gamma[(1 - \hat{\alpha})^3 - (1 - \hat{\alpha})]\}\exp(-ipm\Delta\lambda), \quad (14)$$

where $\gamma = \gamma(m\Delta\lambda)$ corresponds to the Fourier response of F'' multiplied by $\Delta\lambda^2/6$ and is given in appendix A for each of the three interpolation schemes.

The associated TLM solution is

$$\delta F(\lambda, t) = \left[\delta_r F_0 + n\left(\frac{dA}{d\hat{\alpha}}\frac{1}{A}\right)\delta\alpha\right]F(\lambda, t), \quad (15)$$

where

$$\frac{dA}{d\hat{\alpha}} = [1 + \gamma(3\hat{\alpha}^2 - 1)]\exp[-i(p + 1)m\Delta\lambda] + \{-1 + \gamma[-3(1 - \hat{\alpha})^2 + 1]\}\exp(-ipm\Delta\lambda).$$

This is equivalent to

$$\delta_r F(\lambda, t) = \left[\delta_r F_0 + \frac{(dA/d\hat{\alpha})}{A\Delta\lambda}\delta\omega t\right]. \quad (16)$$

This expression is the numerical equivalent of (10), where $(dA/d\hat{\alpha})(1/A)$ represents a discretized first-order spatial derivative operation. In the next section, we will describe the first-order linearization error associated with the second term in the right-hand side of (16) when using interpolation schemes that do not have continuous first-order derivatives at grid points. The question is then whether or not this has an impact on the limit of validity of the TLM for semi-Lagrangian advection schemes. If so, does this problem arise for all interpolation schemes and in which circumstances?

4. Linearization error associated with a semi-Lagrangian passive advection scheme

Let the solution be written as $F = F(\lambda, t; F_0, \alpha) \equiv F(F_0, \alpha)$ to show the dependency of the solution on the initial conditions F_0 and the velocity field. For convenience, variations in the Courant number $\delta\alpha = \delta\omega\Delta t/\Delta\lambda$ associated with $\delta\omega$ are used. The nonlinear difference caused by variations δF_0 and $\delta\alpha$ is then

$$\Delta F = F(F_0 + \delta F_0, \alpha + \delta\alpha) - F(F_0, \alpha),$$

while the TLM approximation to this difference is denoted by δF. In this section, the error made by the tangent linear approximation is studied.

When exact interpolation is used, the nonlinear difference is

$$\Delta F(\lambda,t)=\left\{(1+\delta_r F_0)\left[\frac{A(\alpha+\delta\alpha,m\Delta\lambda)}{A(\alpha,m\Delta\lambda)}\right]^n-1\right\}F(\lambda,t)$$
$$=[(1+\delta_r F_0)\exp(-im\delta\omega t)-1]F(\lambda,t). \quad (17)$$

The discrepancy between the nonlinear difference and the associated tangent linear approximation [given by (10)] is the sum of the second- and higher-order terms

$$\Delta F-\delta F=\left[-\delta_r F_0(im)\delta\omega t+\frac{(im)^2\delta\omega^2t^2}{2}\right]F(\lambda,t)$$
$$+\text{(higher-order terms)}. \quad (18)$$

Referring to Fig. 1, the perturbed upstream point ($\xi+\delta\xi$) is taken to be within the interval $[(I-q-1)\Delta\lambda, (I-q)\Delta\lambda]$ so that $\xi+\delta\xi=(I-q)\Delta\lambda-(\hat{\alpha}+\delta\hat{\alpha})\Delta\lambda$. When numerical interpolation is considered, the discrepancy between the nonlinear difference and the associated TLM solution given by (16) can be written as

$$\frac{\Delta F(\lambda,t)}{F(\lambda,t)}-\frac{\delta F}{F}=c_0+(\ell_1\delta_r F_0+\ell_2\delta\omega t)$$
$$+(q_1\delta_r F_0\delta\omega t+q_2\delta\omega^2t^2)$$
$$+\text{(higher-order terms)}, \quad (19)$$

where

$$c_0=\left\{\left[\frac{A(\hat{a})}{A(\hat{\alpha})}\right]^n-1\right\},$$
$$\ell_1=\left\{\left[\frac{A(\hat{a})}{A(\hat{\alpha})}\right]^n-1\right\},$$
$$\ell_2=\left\{\left[\frac{A(\hat{a})}{A(\hat{\alpha})}\right]^{n-1}\left[\frac{dA(\hat{a})/d\hat{a}}{A(\hat{\alpha})\Delta\lambda}\right]-\left[\frac{dA(\hat{\alpha})/d\hat{\alpha}}{A(\hat{\alpha})\Delta\lambda}\right]\right\},$$
$$q_1=\left[\frac{A(\hat{a})}{A(\hat{\alpha})}\right]^{n-1}\left[\frac{dA(\hat{a})/d\hat{a}}{A(\hat{\alpha})\Delta\lambda}\right],$$
$$q_2=\frac{1}{2n\Delta\lambda^2}\left[\frac{A(\hat{a})}{A(\hat{\alpha})}\right]^{n-1}\frac{1}{A(\hat{\alpha})}$$
$$\times\left\{\frac{d^2A}{d\hat{a}^2}(\hat{a})+\frac{1}{A(\hat{a})}\left[\frac{dA}{d\hat{a}}(\hat{a})\right]^2(n-1)\right\},$$

with $\hat{a}\Delta\lambda=-\xi+(I-q)\Delta\lambda=(p-q)\Delta\lambda+\hat{\alpha}\Delta\lambda$ referring to the distance between ξ and the point $(I-q)\Delta\lambda$ (see Fig. 1). To simplify the notation, $A(\hat{a})\equiv A(q,\hat{a},m\Delta\lambda)$ and $A(\hat{\alpha})\equiv A(p,\hat{\alpha},m\Delta\lambda)$.

The two situations that are likely to be met most of the time occur when ξ and $\xi+\delta\xi$ lie in the same interval ($p-q=0$) or in adjacent intervals ($|p-q|=1$). In the polar regions, however, $\Delta\lambda$ becomes smaller and the displacement could take ($\xi+\delta\xi$) further than one grid interval away from ξ. The argument presented here can be extended to cover such situations. As can be seen from the coefficients appearing in (19) or Eq. (15) of Polavarapu et al. (1996a), it is then necessary to take into account differences of both the values and the first-order derivatives of the perturbed and unperturbed interpolating functions. Investigation of this case is currently under way in the context of the global grid-point shallow-water model of Côté et al. (1993).

a. Case where $p-q=0$

The definition of $\hat{a}$ given above is such that

$$\delta\xi=(\hat{a}-\hat{\alpha})\Delta\lambda-\delta\hat{\alpha}\Delta\lambda.$$

When $q=p$, $\hat{a}\Delta\lambda=\hat{\alpha}\Delta\lambda$ so that $\delta\xi=-\delta\hat{\alpha}\Delta\lambda$ as it should. The coefficients c_0, ℓ_1, and ℓ_2 all vanish and only the quadratic terms remain.

b. Case where $p-q=-1$

Given a perturbed displacement $\delta\xi=-\delta\omega\Delta t$, this situation can be encountered only if $|\hat{a}\Delta\lambda|<\delta\omega\Delta t$. As $\Delta t\to 0$ or $\delta\omega\to 0$, the upstream point ξ would then converge toward a grid point that corresponds to case 2 of Polavarapu et al. (1996a). Here, the focus will be on the characterization of the linearization error for a given $\delta\xi$ as ξ gets closer to $(I-q)\Delta\lambda$. In terms of $\hat{a}$ and $\hat{\alpha}$, this corresponds to the limit $\hat{a}\to 0$ and $\hat{\alpha}\to 1$. In this case, we have

$$\lim_{\substack{\hat{a}\to 0\\ \hat{\alpha}\to 1}} c_0=\left[\frac{A(q,0,m\Delta\lambda)}{A(p,1,m\Delta\lambda)}\right]^n-1=0$$

since the gridpoint values used in the interpolation formulas are uniquely defined. In the same limit, the first-order terms are such that

$$\lim_{\substack{\hat{a}\to 0\\ \hat{\alpha}\to 1}}\ell_2\delta\omega t=\frac{1}{A(p,1,m\Delta\lambda)\Delta\lambda}$$
$$\times\left[\frac{dA}{d\hat{a}}(q,0,m\Delta\lambda)-\frac{dA}{d\hat{\alpha}}(p,1,m\Delta\lambda)\right]\delta\omega t \quad (20)$$

and cancel out only if the interpolation scheme imposes continuity of the first-order derivatives at the grid point. Of the three interpolation schemes considered here, only the cubic spline meets this condition, that is, $\ell_2=0$. Linear interpolation is such that $\ell_2=(im)^2\Delta\lambda$, while the cubic Lagrange yields $\ell_2=-(im)^4\Delta\lambda^3/6$.

Finally, the quadratic terms have the following limiting values:

$$\lim_{\substack{\hat{a}\to 0\\ \hat{\alpha}\to 1}} q_1 = \left[\frac{dA(q,\,0,\,m\Delta\lambda)/d\hat{a}}{A(p,\,1,\,m\Delta\lambda)\Delta\lambda}\right],$$

$$\lim_{\substack{\hat{a}\to 0\\ \hat{\alpha}\to 1}} q_2 = \frac{1}{2n\Delta\lambda^2}\left[\frac{A(q,\,0,\,m\Delta\lambda)}{A(p,\,1,\,m\Delta\lambda)}\right]^{n-1}\frac{1}{A(p,\,1,\,m\Delta\lambda)}$$
$$\times\left\{\frac{d^2A}{d\hat{a}^2}(q,\,0,\,m\Delta\lambda) + \frac{1}{A(q,\,0,\,m\Delta\lambda)} \times\left[\frac{dA}{d\hat{a}}(q,\,0,\,m\Delta\lambda)\right]^2(n-1)\right\}. \quad (21)$$

Referring to appendix A, it is seen that $q_1 = -im$ for all three interpolation schemes (linear, cubic Lagrange, and cubic spline), while

$$q_2 = (im)^2\left(\frac{n-1}{2n} + \frac{1}{2n}\right) \equiv \frac{(im)^2}{2}$$

for the cubic Lagrange and cubic spline. For the linear interpolation, however, it reduces to

$$q_2 = (im)^2\left(\frac{n-1}{2n}\right)$$

because it cannot represent variations in the initial conditions associated with the second-order derivative included in the cubic interpolations. The linearization errors expressed by (20) and (21) are generalizations of those obtained in Polavarapu et al. (1996a) for a single time step ($n = 1$).

Finally, we look at the nature of the error when ξ is close to a grid point but not exactly on it. This means that $1 - \hat{\alpha} = \epsilon$ with $\epsilon \ll 1$, which implies then that $\hat{a} = -\epsilon$. Expanding c_0 in a Taylor series around $\hat{\alpha} = 1$ and $\hat{a} = 0$ leads to

$$c_0 = -\epsilon\frac{\partial c_0}{\partial\hat{a}}\bigg|_{\substack{\hat{a}=0\\ \hat{\alpha}=1}} - \epsilon\frac{\partial c_0}{\partial\hat{\alpha}}\bigg|_{\substack{\hat{a}=0\\ \hat{\alpha}=1}} = (\hat{\alpha}-1)n\Delta\lambda\ell_2$$

with ℓ_2 defined by (20). To leading order, the linearization error reads as

$$\left(\frac{\Delta F}{F} - \frac{\delta F}{F}\right) = \ell_2[(\hat{\alpha}-1)\Delta\lambda n + \delta\omega t] = \ell_2 t\left[(\hat{\alpha}-1)\frac{\Delta\lambda}{\Delta t} + \delta\omega\right] + \text{(higher-order terms)}. \quad (22)$$

As mentioned earlier, ℓ_2 will not vanish for linear or cubic Lagrange interpolations. Since $0 < \hat{\alpha} \leq 1$, (22) indicates that the amplitude of the error is maximal when $\hat{\alpha} = 1$, that is, when the upstream point lands exactly on a grid point [case 2 of Polavarapu et al. (1996a)].

Figure 2 illustrates the nonlinear difference $\|\Delta F/F_0\|$ on the left-hand side and the relative linearization error $\|(\Delta F - \delta F)/\Delta F\|$ on the right-hand side. It has been assumed that $\delta\omega = 0.1\omega$ and that $\delta_t F_0 = 0$. The case of exact interpolation is represented altogether with the three interpolation schemes discussed above. Figure 2 can be interpreted as the results of time integrations over a fixed time period t using monochromatic initial conditions with different wavenumbers. Values of $\Delta\lambda$, ω, and t needed to generate Fig. 2 correspond to the ones used in the first experiment described in section 5. The vertical axis is associated with the nondimensional wavenumber $m\Delta\lambda/\pi$, while the horizontal axis shows the variation with the Courant number α. If $\Delta\lambda$ and ω are taken to be fixed, increasing α then corresponds to increasing the time step. For the case with exact interpolation, Fig. 2 shows that ΔF is independent of the time step while the amplitude of the linearization error increases linearly with m which is in agreement with (10) and (17). The linearization error is also seen to be independent of the time step.

It is well known that for semi-Lagrangian schemes, the interpolation introduces a damping of the solution that is enhanced for smaller time steps because the interpolation is applied more often. Looking at the left panels of Fig. 2, the effect of this damping on the nonlinear difference can indeed be seen to be significantly more important when $\alpha < 1$. By comparison to the exact case, Fig. 2 shows also why a linear interpolation should not be used: its damping is felt on too wide a range of wavenumbers. Finally, one can notice that the cubic spline is less dissipative than the cubic Lagrange.

This damping even leads to negligibly small values of ΔF in the smaller scales when $\alpha < 1$. To avoid division by zero, the relative linearization errors shown on the right panels has been arbitrarily set to 1 whenever $\|\Delta F/F_0\| < 0.001$. The main feature is the discontinuity in the linearization error when the upstream point lies exactly on a grid point (integral values of α). As discussed earlier, this occurs only for the linear and cubic Lagrange interpolation schemes. The results illustrate that this discontinuity is most important when α takes integral values but they also show that the effect persists over a finite range of values of α, which corresponds to $\delta\omega\Delta t$. Consequently, it would get wider as α increases (larger time steps) but it could also be made wider by increasing $\delta\omega$: this would correspond to larger wind perturbations.

The cubic spline does not have this problem and its linearization error agrees well with the estimate of the exact case for wavenumbers smaller than approximately 0.5. If we arbitrarily define 0.25 as the tolerable limit for this ratio, exact and higher-order interpolation schemes respect this limit for waves with $m\Delta\lambda/\pi < 0.3$. The linear interpolation reduces the admissible waves to $m\Delta\lambda < 0.1$ near integral values of α.

It can be seen from (10) and (17) that ΔF and the relative linearization error $E = \|(\Delta F - \delta F)/\Delta F\|$ are proportional to $m\delta\omega T$, where $t = T$ is the integration

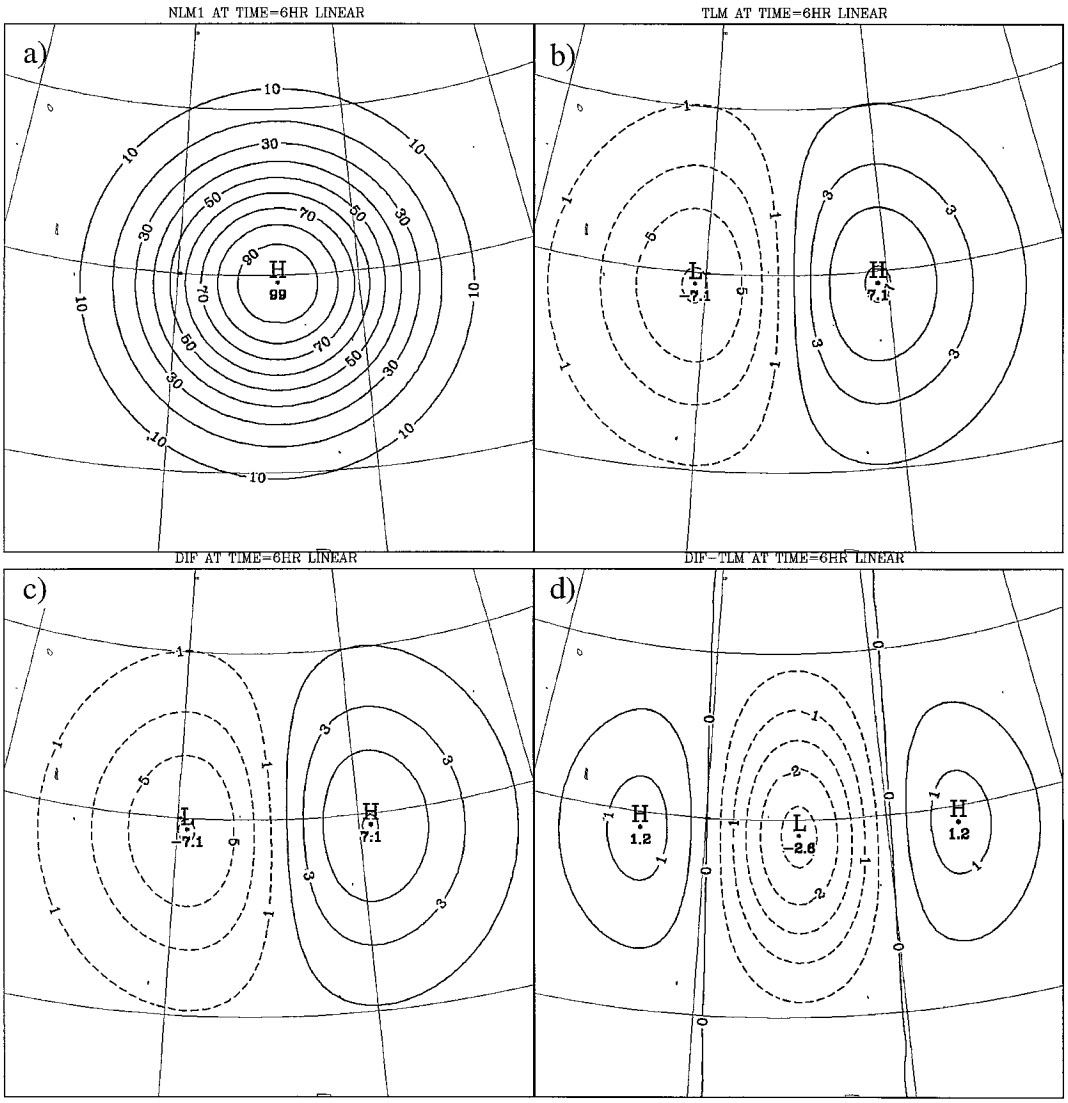

FIG. 3. First solid-body rotation experiment. Here, $L = 5000$ km. Heights corresponding to (a) unperturbed nonlinear run, (b) TLM, (c) nonlinear difference, and (d) discrepancy between the last two. At the end of the 6-h period for linear interpolation. The contour intervals are 10 (NLM1), 2 (TLM and DIF), and 0.5 (DIF − TLM).

period used to produce Fig. 2. Referring to the bottom panels of Fig. 2, if $E < 0.25$ still defines the limit of validity of the TLM, doubling the integration time ($t = 2T$) would result in having the TLM valid only for $0 < m\Delta\lambda/\pi < 0.15$, a more restricted range. Similarly, halving the integration interval would make the TLM valid over an extended range of wavenumbers ($0 < m\Delta\lambda/\pi < 0.6$). If $\Delta\lambda$ is increased (e.g., $\Delta\lambda_2 = 2\Delta\lambda$), ΔF and E are found for $m\Delta\lambda_2$ by referring to the bottom panels of Fig. 2 at $m\Delta\lambda = m\Delta\lambda_2/2$.

In the next section, we will use these results to define experiments of passive tracer advection that will reveal the nature of the linearization error associated with the three interpolation schemes.

5. Limit of validity of the tangent linear approximation

In this section, (1) is integrated with a semi-Lagrangian scheme based on the different interpolations discussed above. To emphasize the problems in the linearization error, experiments are done first with a wind field prescribed to be that associated with the solid-body rotation. By adjusting the angular velocity, it is then possible to maintain values of $\alpha \sim 1$. The second set of experiments will use a TLM defined trajectory with respect to a spatially varying wind field obtained from a shallow-water model integration. In that case, the criterion of having $\alpha \sim 1$ occurs with a vanishingly small probability.

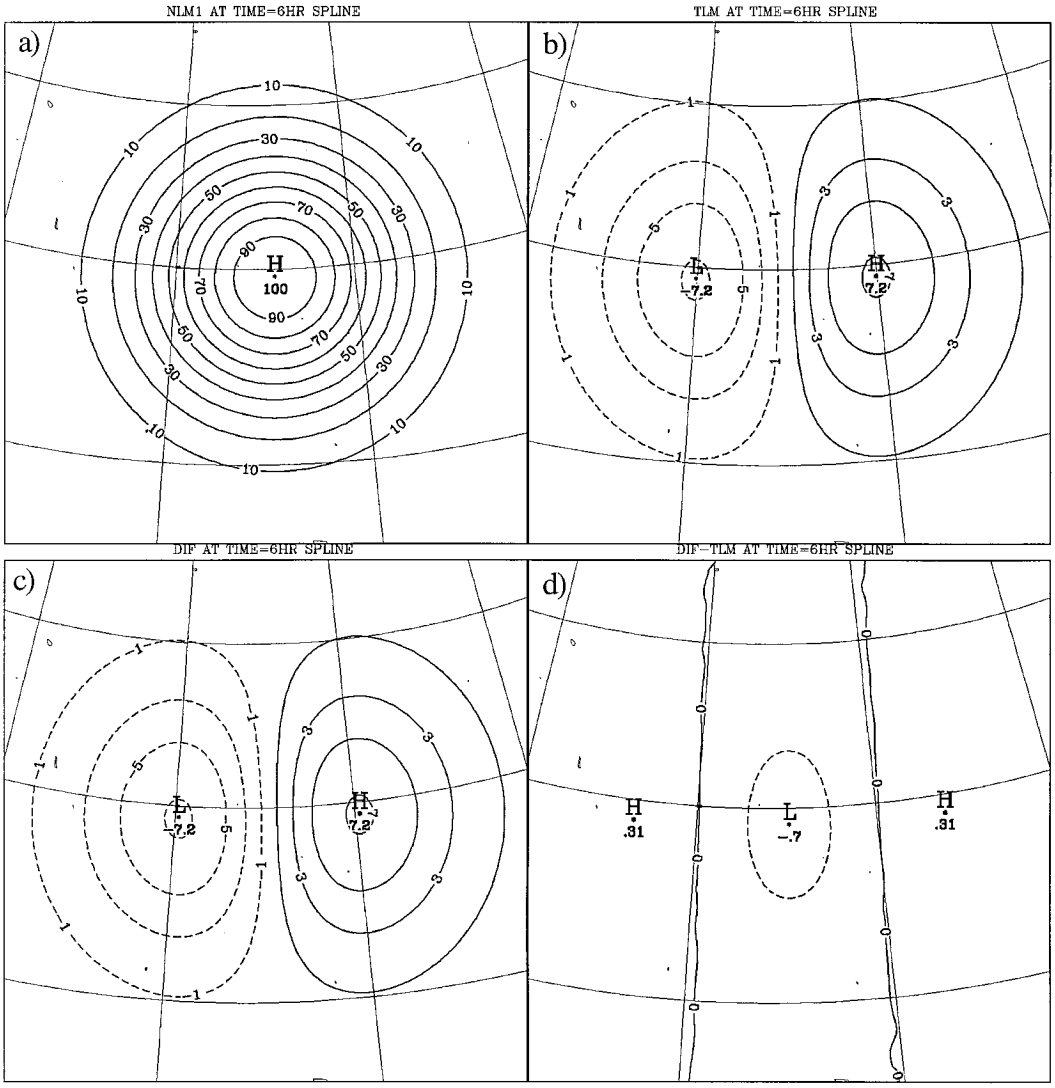

FIG. 4. As in Fig. 3 except for cubic spline interpolation.

Returning to the vector form of the two-dimensional advection equation (1) and using a centered approximation for the semi-Lagrangian derivative yields

$$\frac{F(\mathbf{r}, t) - F(\mathbf{r}^-, t - \Delta t)}{\Delta t} = 0, \tag{23}$$

where the position at forecast time t is chosen to be a grid point $\mathbf{r}$ and the forecast value at this point is found by determining the value of F at the upstream location $\mathbf{r}^-$ at old time $t - \Delta t$. The associated TLM is

$$\frac{\delta F(\mathbf{r}, t) - \delta F(\bar{\mathbf{r}}^-, t - \Delta t) - \nabla F(\bar{\mathbf{r}}^-, t - \Delta t)\cdot\delta\mathbf{r}^-}{\Delta t} = 0, \tag{24}$$

where the overbar refer to mean state values. In the case of solid-body rotation, the upstream positions $\mathbf{r}^-$ on the sphere in the original (λ, θ) system needed for interpolation in (23) and (24) and perturbations $\delta\mathbf{r}^-$ are evaluated exactly using (3)–(5) of Ritchie (1987) based on the relations between the two spherical coordinates system (λ', θ') and (λ, θ) defined in section 2. These evaluations together with their associated TLM are given in appendix B. The initial field is chosen to be a ''Gaussian hill'' as in Ritchie (1987) together with a grid resolution $\Delta\lambda = 1°$ and a time step $\Delta t = 1$ h for solid-body rotation and tracer experiments. By setting the velocity to be constant, the problem becomes similar to the situation described in section 4. In fact, the parameters of the present problem have been set so that it corresponds to the situation described in Fig. 2.

To illustrate the linearization error introduced when $\alpha \sim 1$, the time step is chosen so that ω corresponds to $\alpha = 0.9$ while $\delta\omega$ is such that $(\alpha + \delta\alpha) = 1.1$. In a first experiment, a Gaussian hill with a half-width of

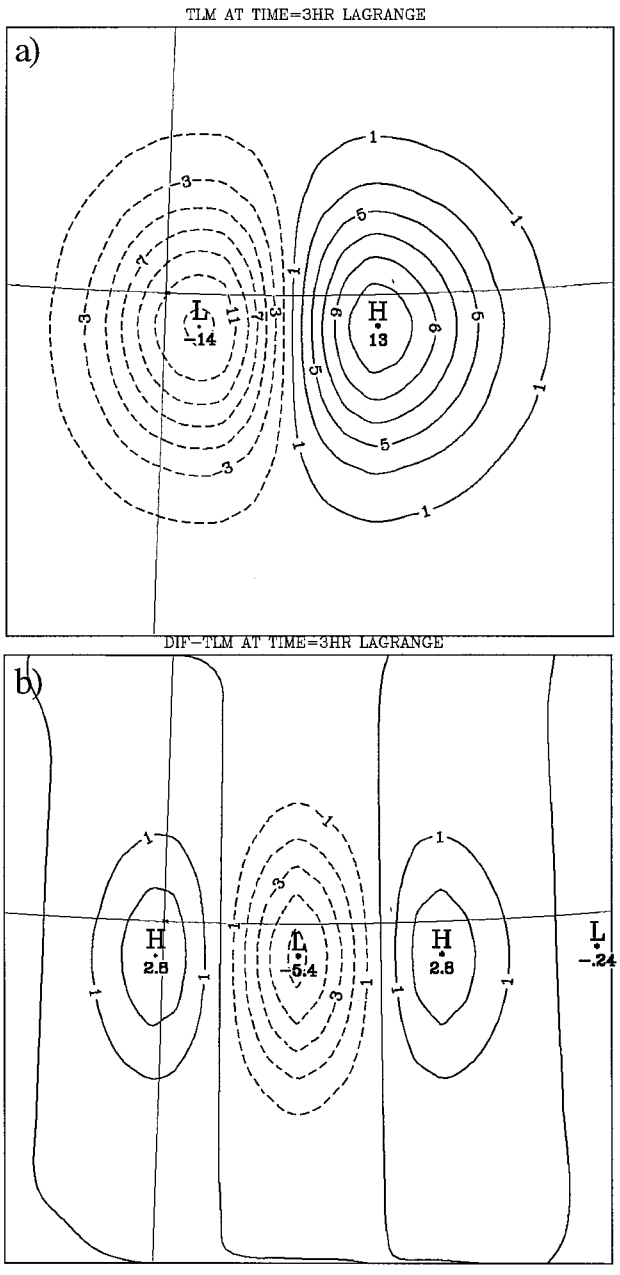

FIG. 5. Second solid-body rotation experiment. Here, $L = 1250$ km. Heights corresponding to (a) TLM and (b) discrepancy between nonlinear difference and TLM. At the end of the 3-h period for cubic Lagrange interpolation. The contour intervals are 2 (TLM) and 1 (DIF − TLM).

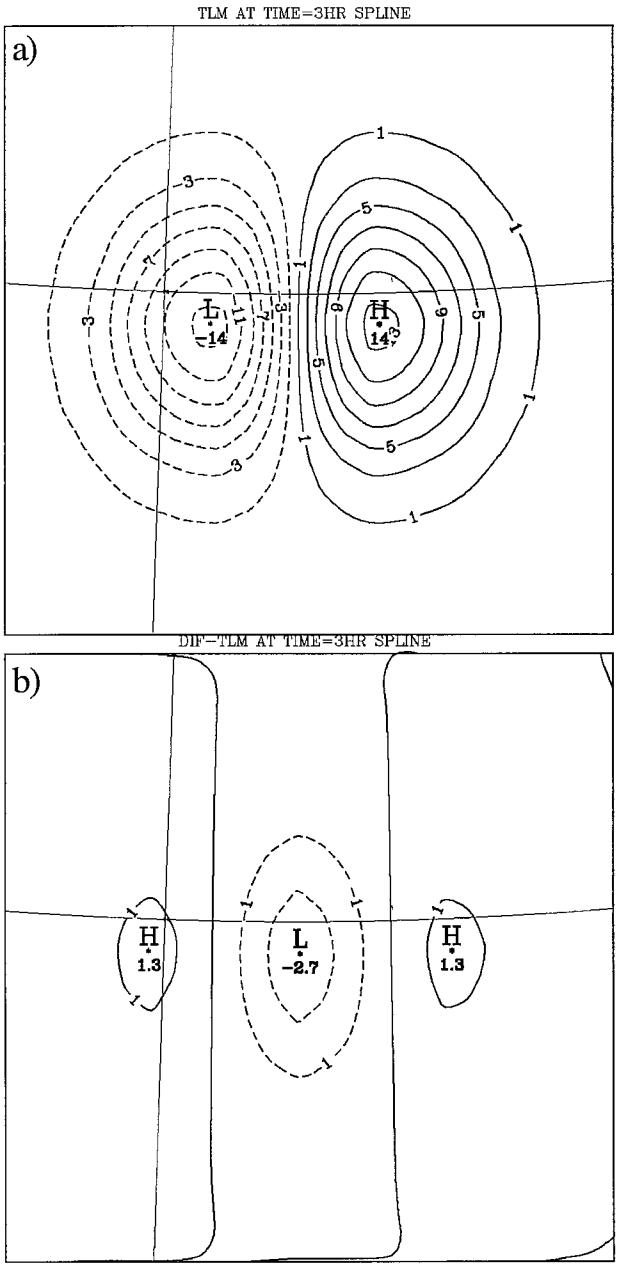

FIG. 6. As in Fig. 5 except for cubic spline interpolation.

5000 km is rotated around the equator and the resulting 6-h integration is shown in Fig. 3 (Fig. 4) when linear (cubic spline) interpolation is used. In section 2, the analytic solution showed that δF is rapidly dominated by the component that grows linearly in time. Referring to (10) and (17), δF and ΔF should approximately correspond to the first derivative of F up to a multiplicative factor (shown in Fig. A1). Figures 3b,c and 4b,c agree very well with the pattern of the first derivative of F. On the other hand, it can also be deduced from (18) that the quadratic term neglected by the tangent linear approximation varies as the second derivative of F. A comparison of Figs. 3d and 4d against Fig. A1 shows that this is indeed the case. There is, however, a significant difference in amplitude that can be related to the linearization error associated with linear interpolation, which introduces a phase error by adding the second-order derivative term appearing in (20).

The results of section 4 lead us to the conclusion that the cubic Lagrange scheme introduces a linearization

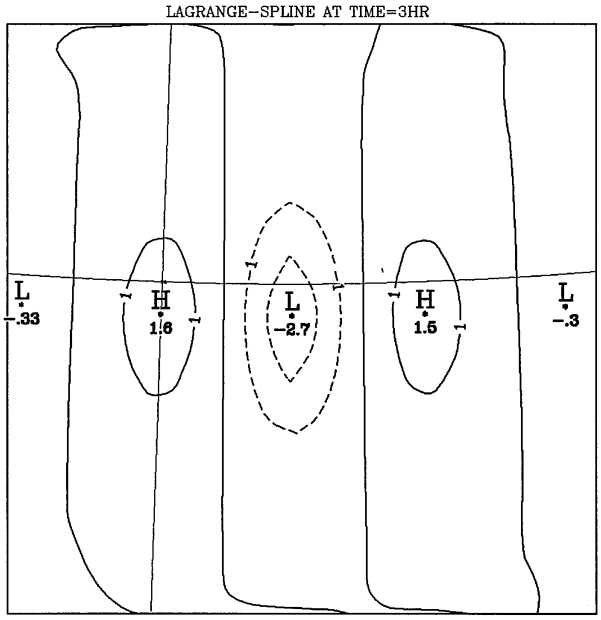

FIG. 7. Second solid-body rotation experiment. Here, $L = 1250$ km. Heights corresponding to difference between linearizations errors (DIF − TLM) of cubic Lagrange and cubic spline interpolations at the end of the 3-h period. The contour interval is 1.

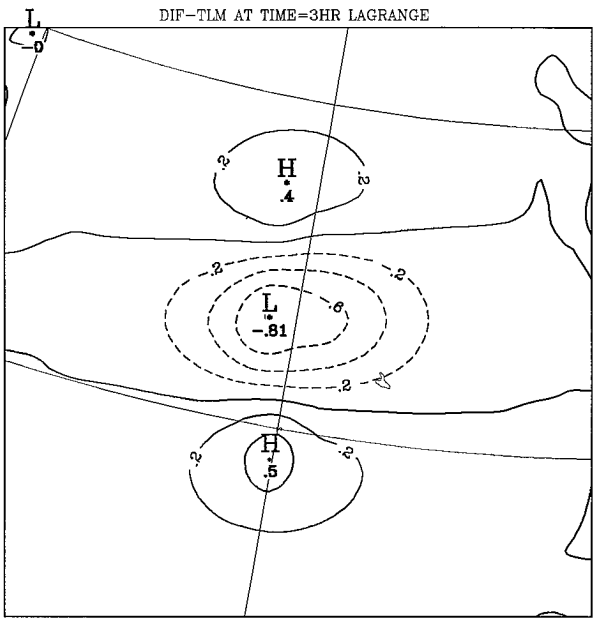

FIG. 8. Third solid-body rotation experiment. Here, $L = 1250$ km. Heights corresponding to the discrepancy between nonlinear difference and TLM. At the end of the 3-h period for cubic Lagrange interpolation. The contour interval is 0.2.

error that is absent when a cubic spline is used. This being more important in the small scales, the characteristic length of the Gaussian hill in the second experiment was reduced to 1250 km and the integration period was reduced to 3 h. All other parameters remained as in the previous experiment. Figures 5b and 6b show that the error made with a cubic Lagrange interpolation is about twice that of the cubic spline. This is due to the fact that the linearization error is proportional to the fourth-order derivative of F [see the discussion following (20)] and adds up to the true error of the TLM that is proportional to the second-order derivative. On the other hand, the error pattern of the cubic spline is representative of the true error of the TLM. The difference between both linearization errors is presented in Fig. 7 and leads to a pattern resembling the negative fourth-order derivative of the advected Gaussian hill.

In a third experiment, minor linearization errors are shown to appear locally where the advecting wind leads to a sustained integral Courant number. The north pole P' of the rotating system is chosen to be at $(\pi, 0)$ on the equator. We induce the rotation of an initial Gaussian hill ($L = 1250$ km) centered at the intersection of the equator and $\pi + 0.35$ rad meridian ($\sim 200°$ longitude). By choosing the angular velocity ω as $\omega \sin[(\pi + 0.35) - \pi] = \Delta\theta/\Delta t$ [based on (10) of Ritchie (1987)], a Courant number near 0.99 is sustained at the $\pi + 0.35$ rad meridian. The perturbation $\delta\omega$ is chosen to be 10% of ω. At the end of the 3-h integration period, Fig. 8 and Fig. 9 illustrate the discrepancy between the nonlinear difference and the TLM for the cubic Lagrange and cubic spline interpolations, respectively. A small discontinuity is present near that meridian when using cubic Lagrange interpolation.

The solid-body rotation experiments were used to emphasize the linearization error committed by the various interpolation schemes. However, this creates an extreme situation because the criterion of having $\alpha \sim 1$ can be

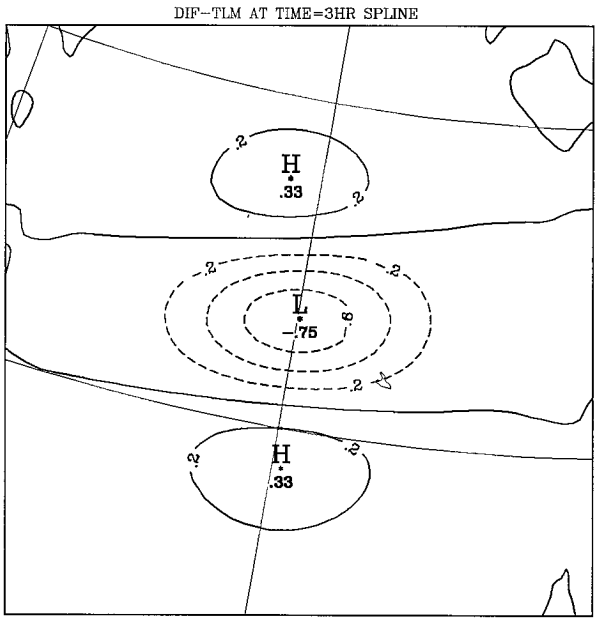

FIG. 9. As in Fig. 8 except for cubic spline interpolation.

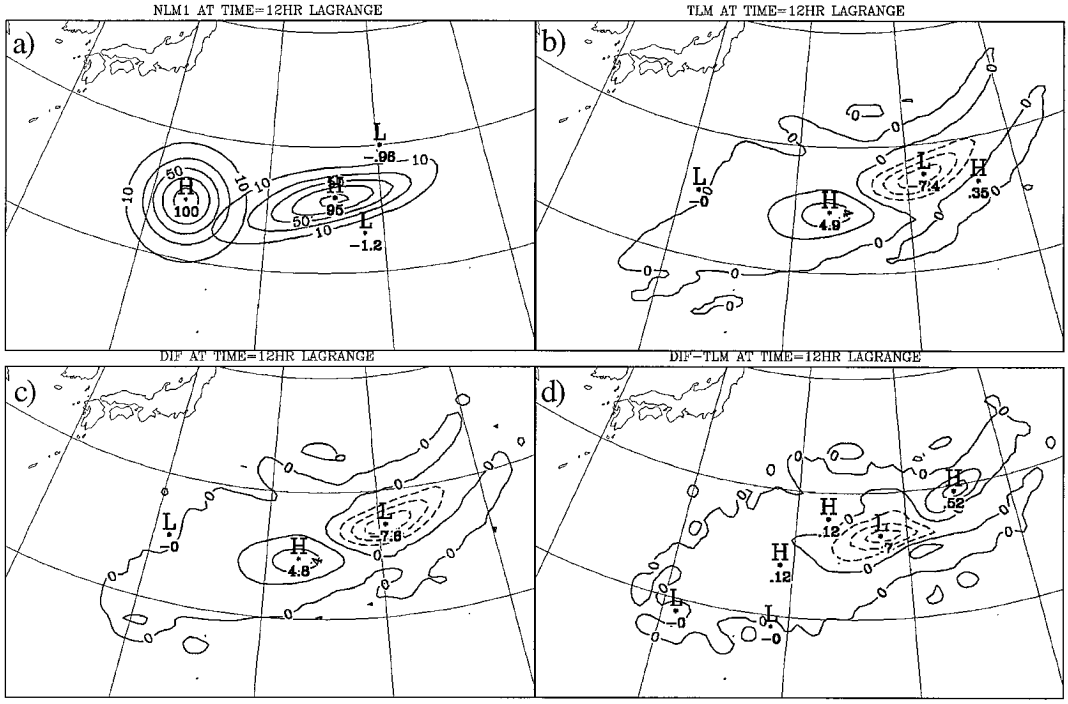

FIG. 10. Tracer experiment. Here, $L = 1250$ km. Heights corresponding to (a) unperturbed nonlinear run, (b) TLM, (c) nonlinear difference, (d) discrepancy between the last two, at the end of the 12 h period for cubic Lagrange interpolation. The initial field is added in panel (a). The contour intervals are 30 (NLM1), 2 (TLM and DIF), and 0.2 (DIF − TLM).

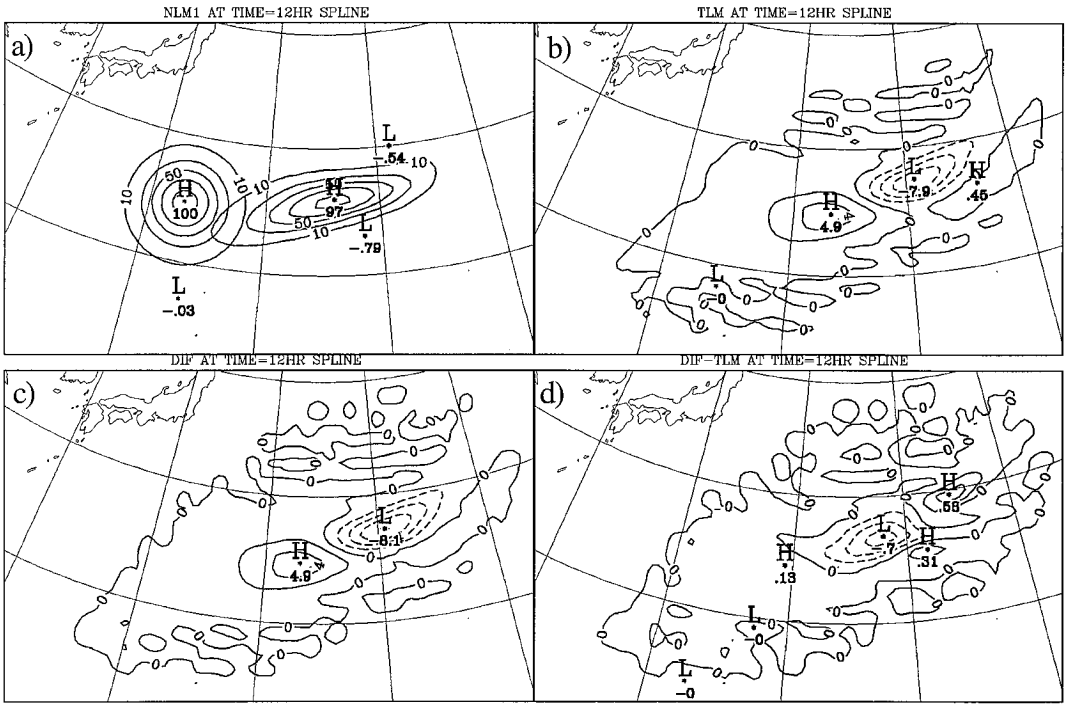

FIG. 11. As in Fig. 10 except for cubic spline interpolation.

maintained at the same location over the entire integration period. To investigate the linearization error in a more realistic configuration, the wind configuration was obtained from an integration of a shallow-water model and used to advect a tracer with an initial Gaussian hill distribution. These integrations are performed for cubic Lagrange and cubic spline interpolation schemes to see the consequence of the linearization error associated with the cubic Lagrange interpolation. Upstream positions $\mathbf{r}^-$ and perturbations $\delta\mathbf{r}^-$ on the sphere are evaluated by iteratively solving the second-order in time trajectory calculations (15)–(18) of Côté and Staniforth (1988). These trajectory calculations together with their associated TLM are given in appendix B. Sufficient iterations were used in order to guarantee convergence. Implication of inadequate convergence on the validity of linearized iterative processes is studied in Polavarapu et al. (1996b).

The winds used here lead to a zonal Courant number between 0.8 and 1.2 and the results of the integrations with cubic Lagrange and cubic spline interpolations are illustrated in Figs. 10 and 11, respectively, at the end of the 12-h period. The heights corresponding to the unperturbed nonlinear run, TLM, nonlinear difference, and discrepancy between the last two are shown. The initial field tracer distribution has been superimposed in the unperturbed nonlinear run panel for convenience. Both schemes have similar linearization errors in the case of a typical situation where the probability of being advected to integral grid points is very small. The difference between the two is very small and similar to that for the case of the solid body rotation.

6. Summary

In this paper, the nature of the linearization error was investigated when small but finite perturbations are integrated over a finite period of time. This extends the study of Polavarapu et al. (1996a), who showed that nondifferentiable operations are introduced in the interpolation part of semi-Lagrangian advection and create a linearization error even for infinitesimal perturbations. Based on an analytical treatment of the 1D advection problem, it was concluded that when the unperturbed and perturbed upstream point lie in the same interval, the linearization error is of second-order and is then within the error made by the TLM approximation itself. However, when those two points lie in different intervals, first-order linearization error terms are present when the interpolation scheme does not admit continuity of the first-order derivative at grid points. This occurs for linear and cubic Lagrange interpolations and was seen to be more pronounced at small scales. First-order linearization error terms were shown to amplify in time and to be maximal for integral Courant numbers. An important conclusion was that this error is introduced not only if the upstream point lies exactly on a grid point as in Polavarapu et al. (1996a) but also if it falls within some finite neighborhood of the grid point. This is therefore an event that occurs with a small but nonzero probability.

To illustrate the nature of the error, we performed integrations in time of a tracer advected by a wind field associated with a solid-body rotation. By properly choosing the constant wind and the time step, it was possible to create the worst case: a situation in which the problematic linearization error is maintained over the entire integration period. The results were in agreement with the analytical results of the 1D case and showed that the error made with a cubic Lagrange interpolation was still present but small if compared to that made by using a linear interpolation. The fact that the linear scheme leads to a problem with the TLM is inconsequential in a sense because its dissipative nature makes it unsuited for semi-Lagrangian schemes. The cubic Lagrange scheme on the other hand is used for semi-Lagrangian integration and it is then of importance to establish if it does create a problem. In reality, the situation where a grid point has its upstream point in the neighborhood of another grid point occurs with a very small probability and not systematically over an entire integration period. By using a realistic wind field varying in space with local Courant numbers between 0.8 and 1.2, the TLM error patterns were seen to be very similar for the integration with a cubic Lagrange or cubic spline interpolation.

The delicate numerics at the poles could have additional implications on the TLM validity where new nondifferentiable operations are present and where the increased size of the displacement variation when approaching polar regions may lead to zero-order linearization errors. Our study is therefore one step toward answering the more general question regarding the sensitivity of the TLM validity to the size of the time step raised in Li et al. (1993) for a more general problem involving semi-Lagrangian advection where accumulated linearization errors are now allowed to feedback to the advecting wind field. Further studies in that direction are currently under way in the context of the TLM of Côté et al. (1993) global gridpoint shallow-water model.

Acknowledgments. The authors are indebted to Jean Côté and Steve Thomas for providing solid-body rotation material. Thanks are also expressed to Hal Ritchie for reviewing the manuscript.

APPENDIX A

Interpolation Schemes

Various interpolation schemes may be obtained from the scheme, (12), simply by choosing how the F'' are calculated. Three examples are given below. This is extracted for convenience from Polavarapu et al. (1996a).

1) Linear interpolation

$$F''_I = 0. \tag{A1}$$

2) Cubic Lagrange interpolation

$$F''_I = \frac{F_{I-1} - 2F_I + F_{I+1}}{\Delta\lambda^2}. \tag{A2}$$

3) Cubic spline interpolation. By enforcing continuity of first derivatives at longitude grid point $\lambda = I\Delta\lambda$ we have

$$\frac{F''_{I+1} + 4F''_I + F''_{I+1}}{6} = \frac{F_{I-1} - 2F_I + F_{I+1}}{\Delta\lambda^2}. \quad \text{(A3)}$$

This tridiagonal system of equations can be solved to simultaneously produce all F''_I. The Fourier response of F'' multiplied by $\Delta\lambda^2/6$ as needed in (14) for each interpolation is

$$\gamma_{\text{lin}} = 0$$

$$\gamma_{\text{cl}} = -\frac{2}{3}\sin^2(0.5m\Delta\lambda)$$

$$\gamma_{\text{cs}} = -\frac{2\sin^2(0.5m\Delta\lambda)}{[\cos(m\Delta\lambda) + 2]}, \quad \text{(A4)}$$

where the subscripts lin, cl, and cs refer to the linear, cubic Lagrange, and cubic spline schemes, respectively.

General expressions for $A(\hat{a})$, $A(\hat{\alpha})$, and derivatives when considering case 2 of Polavarapu et al. (1996a) are

$$\frac{A(\hat{a})}{A(\hat{\alpha})} = 1$$

$$\frac{dA(\hat{a})/d\hat{a} - dA(\hat{\alpha})/d\hat{\alpha}}{A(\hat{\alpha})\Delta\lambda} = 2\left[\frac{(1-\gamma)\cos(m\Delta\lambda) - (1+2\gamma)}{\Delta\lambda}\right]\text{sgn}(q-p)$$

$$\frac{dA(\hat{a})/d\hat{a}}{A(\hat{\alpha})\Delta\lambda} = \left\{\frac{(1-\gamma)\exp\left(-im\Delta\lambda\dfrac{dp}{|dp|}\right) - (1+2\gamma)}{\Delta\lambda}\right\}\text{sgn}(q-p)$$

$$\frac{d^2A(\hat{a})/d\hat{a}^2}{A(\hat{\alpha})\Delta\lambda^2} = \frac{6\gamma}{\Delta\lambda^2}. \quad \text{(A5)}$$

The limiting values of expressions as $\Delta\lambda$ goes to zero for the aforementioned schemes are

$$\frac{dA(\hat{a})/d\hat{a} - dA(\hat{\alpha})/d\hat{\alpha}}{A(\hat{\alpha})\Delta\lambda} \cong \begin{cases} (im)^2\Delta\lambda\ \text{sgn}(q-p), & \text{linear} \\ -\dfrac{(im)^4}{6}\Delta\lambda^3\ \text{sgn}(q-p), & \text{cubic Lagrange} \\ 0, & \text{cubic spline} \end{cases}$$

$$\frac{dA(\hat{a})/d\hat{a}}{A(\hat{\alpha})\Delta\lambda} \cong -(im), \quad \text{for all interpolations}$$

$$\frac{d^2A(\hat{a})/d\hat{a}^2}{A(\hat{\alpha})\Delta\lambda^2} \cong \begin{cases} 0, & \text{linear} \\ (im)^2, & \text{cubic Lagrange} \\ (im)^2, & \text{cubic spline.} \end{cases} \quad \text{(A6)}$$

Finally, the Gaussian Hill and its derivatives are illustrated in Fig. A1 ($L = 1250$ km.)

APPENDIX B

Upstream Position Calculations

In the case of solid-body rotation, the upstream positions $\mathbf{r}^-$ and perturbations $\delta\mathbf{r}^-$ on the sphere in the original (λ, θ) system needed in (23)–(24) are evaluated exactly using (3)–(5) of Ritchie (1987) based on the relations between the two spherical coordinates system (λ', θ') and (λ, θ) defined in section 2. These evaluations are recalled for convenience;

$$\sin\theta' = \sin\theta\sin\theta_0 + \cos\theta\cos\theta_0 \times \cos(\lambda - \lambda_0)$$

$$\sin\theta = \sin\theta'\sin\theta_0 - \cos\theta'\cos\theta_0\cos\lambda'$$

$$\cos\theta'\sin\lambda' = \cos\theta\sin(\lambda - \lambda_0). \quad \text{(B1)}$$

The associated TLM is therefore

$$\cos\theta'\delta\theta' = \cos\theta\delta\theta\sin\theta_0 - \sin\theta\delta\theta\cos\theta_0\cos(\lambda - \lambda_0) - \cos\theta\cos\theta_0\sin(\lambda - \lambda_0)\delta\lambda$$

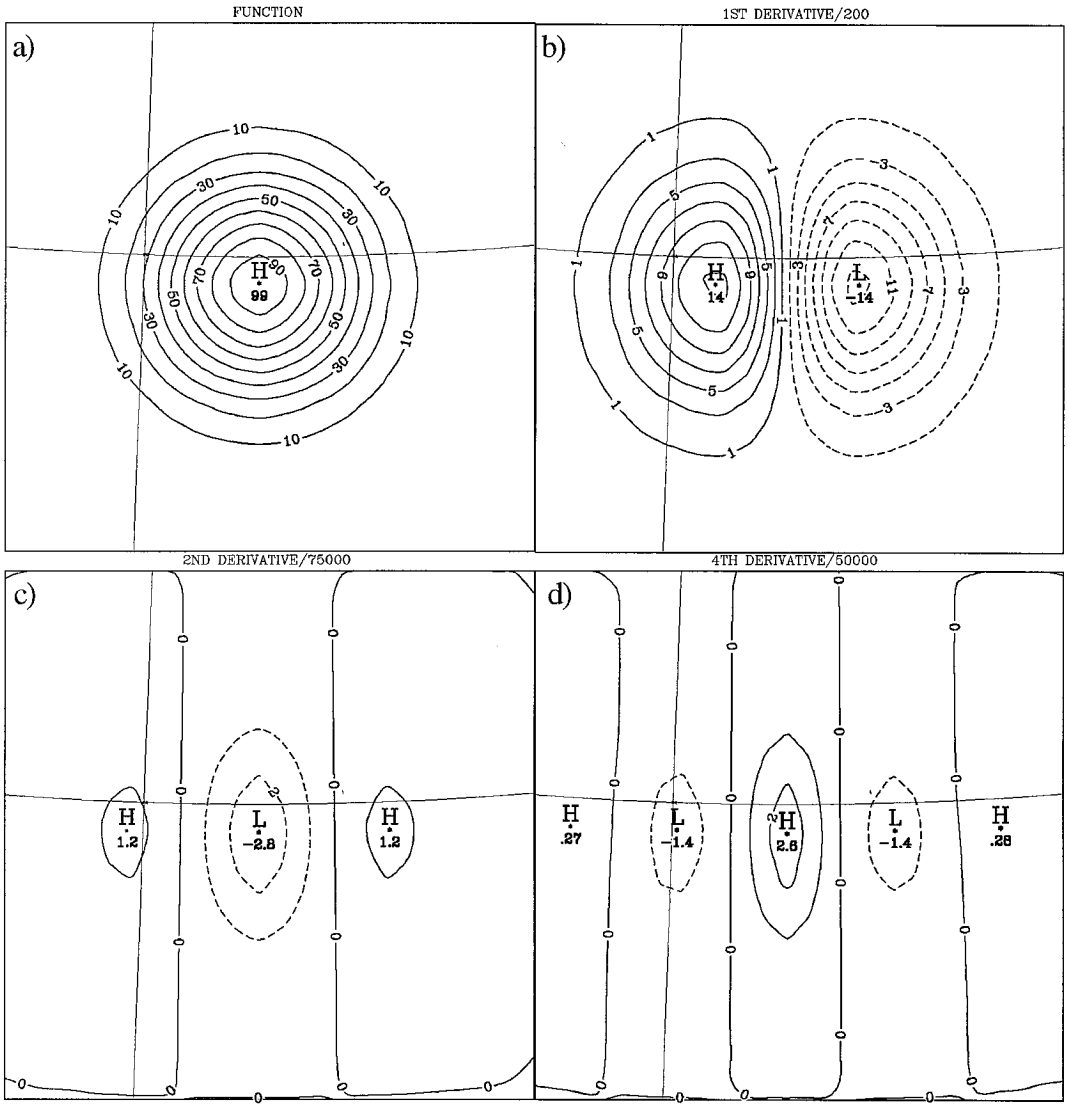

FIG. A1. Heights of a Gaussian hill (L = 1250 km) and its derivatives. The contour intervals are 10 (FUNCTION), 2 (1ST DERIVATIVE/200), 1 (2ND DERIVATIVE/75000), and 1 (4TH DERIVATIVE/50000).

$$\begin{aligned}\cos\theta\delta\theta &= \cos\theta'\delta\theta'\sin\theta_0 + \sin\theta'\delta\theta'\cos\theta_0\cos\lambda' \\ &\quad + \cos\theta'\cos\theta_0\sin\lambda'\delta\lambda' \\ -\sin\theta'\delta\theta'\sin\lambda' &+ \cos\theta'\cos\lambda'\delta\lambda' \\ &= -\sin\theta\delta\theta\,\sin(\lambda-\lambda_0) + \cos\theta\cos(\lambda-\lambda_0)\delta\lambda,\end{aligned} \tag{B2}$$

where $\delta\lambda' = -\delta\omega\Delta t$ and $\delta\theta' = 0$ in our case.

Upstream positions $\mathbf{r}^-$ and perturbations $\delta\mathbf{r}^-$ on the sphere needed in (23) and (24) for a semi-Lagrangian passive tracer integration driven by shallow water integrated winds are evaluated by iteratively solving second-order in time trajectory calculations (15)–(18) of Côté and Staniforth (1988). These trajectory calculations are recalled for convenience.

Suppose a fluid element is at position $\mathbf{r}$ at time t. To find the upstream location $\mathbf{r}^-(t-\Delta t)$ at time $t-\Delta t$, we first find the upstream position $\mathbf{r}^0(t-\Delta t/2)$ at time $t-\Delta t/2$ by iteratively solving

$$\mathbf{r}^0 = \cos\theta\mathbf{r} + \sin\theta\mathbf{r}\times\frac{\mathbf{r}\times\mathbf{V}^0}{|\mathbf{r}\times\mathbf{V}^0|}, \tag{B3}$$

where

$$\mathbf{V}^0 = \mathbf{V}\left(\mathbf{r}^0,\, t-\frac{1}{2}\Delta t\right) \tag{B4}$$

$$\theta = \frac{|\mathbf{V}^0|}{a}\frac{\Delta t}{2}. \tag{B5}$$

Geometrically, we search for a point $\mathbf{r}^0$ situated a distance $1/2|\mathbf{V}^0|\Delta t$ upstream on the sphere, such that $\mathbf{r}$, $\mathbf{r}^0$, and $\mathbf{V}^0$ are coplanar. The point $\mathbf{r}^-$ is then

$$\mathbf{r}^- = 2(\mathbf{r}\cdot\mathbf{r}^0)\mathbf{r}^0 - \mathbf{r}. \tag{B6}$$

We find the perturbation $\delta\mathbf{r}^0(t - \Delta t/2)$ in upstream position at time $t - \Delta t/2$ by iteratively solving

$$\delta\mathbf{r}^0 = -\sin\bar{\theta}\delta\theta\mathbf{r} + \cos\bar{\theta}\delta\theta\mathbf{r}\times\frac{\mathbf{r}\times\bar{\mathbf{V}}^0}{|\mathbf{r}\times\mathbf{V}^0|} - \sin\bar{\theta}\mathbf{r} \times\left[\frac{(\mathbf{r}\times\bar{\mathbf{V}}^0)\cdot(\mathbf{r}\times\delta\mathbf{V}^0)}{|\mathbf{r}\times\bar{\mathbf{V}}^0|^2}\right]\frac{\mathbf{r}\times\bar{\mathbf{V}}^0}{|\mathbf{r}\times\bar{\mathbf{V}}^0|}, \tag{B7}$$

where the barred quantities refer to mean state and

$$\delta\mathbf{V}^0 = \delta\mathbf{V}\left(\bar{\mathbf{r}}^0, t - \frac{1}{2}\Delta t\right) + \bar{\nabla}\bar{\mathbf{V}}\left(\bar{\mathbf{r}}^0, t - \frac{1}{2}\Delta t\right)\cdot\delta\mathbf{r}^0 \tag{B8}$$

$$\delta\theta = \frac{\bar{\mathbf{V}}^0\cdot\delta\mathbf{V}^0}{|\bar{\mathbf{V}}^0|a}\frac{\Delta t}{2}. \tag{B9}$$

The perturbation $\delta\mathbf{r}^-$ is then

$$\delta\mathbf{r}^- = 2(\mathbf{r}\cdot\delta\mathbf{r}^0)\bar{\mathbf{r}}^0 + 2(\mathbf{r}\cdot\bar{\mathbf{r}}^0)\delta\mathbf{r}^0. \tag{B10}$$

REFERENCES

Bao, J.-W., and Y.-H. Kuo, 1995: On–off switches in the adjoint method: Step functions. *Mon. Wea. Rev.*, **123,** 1589–1594.

Bates, J. R., and A. McDonald, 1982: Multiply-upstream, semi-Lagrangian advective schemes: Analysis and application to a multilevel primitive equation model. *Mon. Wea. Rev.*, **110,** 1831–1842.

Côté, J., and A. Staniforth, 1988: A two-time-level semi-Lagrangian semi-implicit scheme for spectral models. *Mon. Wea. Rev.*, **116,** 2003–2012.

——, M. Roch, A. Staniforth, and L. Fillion, 1993: A variable-resolution semi-Lagrangian finite-element global model of the shallow-water equations. *Mon. Wea. Rev.*, **121,** 231–243.

Courtier, P., J. Derber, R. Errico, J.-F. Louis, and T. Vukicevic, 1993: Important literature on the use of adjoint, variational methods, and the Kalman filter in meteorology. *Tellus,* **45A,** 342–357.

Daley, R., 1995: Estimating the wind field from chemical constituent observations: Experiments with a one-dimensional extended Kalman filter. *Mon. Wea. Rev.,* **123,** 181–198.

Evensen, G., 1992: Using the Extended Kalman Filter with a multilayer quasi-geostrophic ocean model. *J. Geophys. Res.*, **97,** 17 905–17 924.

Gauthier, P., P. Courtier, and P. Moll, 1993: Assimilation of simulated wind Lidar data with a Kalman filter. *Mon. Wea. Rev.*, **121,** 1803–1820.

Lacarra, J.-F., and O. Talagrand, 1988: Short-range evolution of small perturbations in a barotropic model. *Tellus,* **40A,** 81–95.

LeDimet, F. X., and O. Talagrand, 1986. Variational algorithms for analysis and assimilation of meteorological observations: Theoretical aspects. *Tellus,* **38A,** 97–110.

Li, Y., I. M. Navon, P. Courtier, and P. Gauthier, 1993: Variational data assimilation with a semi-Lagrangian semi-implicit global shallow-water equation model and its adjoint. *Mon. Wea. Rev.*, **121,** 1759–1769.

McDonald, A., 1984: Accuracy of multiply-upstream, semi-Lagrangian advective schemes. *Mon. Wea. Rev.*, **112,** 1267–1275.

Ménard, R., 1994: Kalman filtering of Burgers' equation and its application to atmospheric data assimilation. Ph.D. dissertation, McGill University, 211 pp. [Available from the Dept. of Atmospheric and Ocean Science, McGill University, 805 Sherbrooke Street West, Montreal, PQ H3A 2K6, Canada.]

Polavarapu, S., M. Tanguay, R. Ménard, and A. Staniforth, 1996a: The tangent linear model for semi-Lagrangian schemes: Linearizing the process of interpolation. *Tellus,* **48A,** 74–95.

——, ——, and A. Staniforth, 1996b: Linearizing iterative processes for 4D data assimilation schemes. Priprints, *Proc. 11th Conf. on Numerical Weather Prediction,* Norfolk, VA, Amer. Meteor. Soc., 243–245.

Pudykiewicz, J., and A. Staniforth, 1984: Some properties and comparative performance of the semi-Lagrangian method of Robert in the solution of the advection-diffusion equation. *Atmos.-Ocean,* **22,** 283–308.

Rabier, F., and P. Courtier, 1992: Four-dimensional assimilation in the presence of baroclinic instability. *Quart. J. Roy. Meteor. Soc.*, **118,** 649–672.

Ritchie, H., 1986: Eliminating the interpolation associated with the semi-Lagrangian scheme. *Mon. Wea. Rev.*, **114,** 135–146.

——, 1987: Semi-Lagrangian advection on a Gaussian grid. *Mon. Wea. Rev.*, **115,** 608–619.

Robert, A., T. L. Yee, and H. Ritchie, 1985: A semi-Lagrangian and semi-implicit numerical integration for multilevel atmospheric models. *Mon. Wea. Rev.*, **113,** 388–394.

Tanguay, M., P. Bartello, and P. Gauthier, 1995: Four-dimensional data assimilation with a wide range of scales. *Tellus,* **47A,** 974–997.

Thépaut, J.-N., P. Courtier, G. Belaud, and G. Lemaître, 1996: Dynamical structure functions in a four-dimensional variational assimilation: A case study. *Quart. J. Roy. Meteor. Soc.*, **122,** 535–561.

Vukicevic, T., 1991: Nonlinear and linear evolution of initial forecast errors. *Mon. Wea. Rev.*, **119,** 1602–1611.

——, and R. M. Errico, 1993: Linearization and adjoint of parameterized moist diabatic processes. *Tellus,* **45A,** 493–510.

Zou, X., I. M. Navon, and J. G. Sela, 1993: Variational data assimilation with moist threshold processes using the NMC spectral model. *Tellus,* **45A,** 370–387.

Zupanski, D., 1993: The effects of discontinuities in the Betts–Miller cumulus convection scheme on four-dimensional variational data assimilation. *Tellus,* **45A,** 511–524.